remote sensing

MDPI

Article

Mine Subsidence Monitoring Integrating DS-InSAR with UAV Photogrammetry Products: Case Studies on Hebei and Inner Mongolia

Jinqi Zhao [1,†], Xuhai Yang [2,†], Zhaojiang Zhang [2,3], Yufen Niu [2,3,*] and Zheng Zhao [4]

[1] School of Environment Science and Spatial Informatics, China University of Mining and Technology, Xuzhou 221116, China; masurq@cumt.edu.cn
[2] School of Mining and Geomatics Engineering, Hebei University of Engineering, Handan 056038, China; 13932005269@163.com (X.Y.); zhangzhaojiang@hebeu.edu.cn (Z.Z.)
[3] Handan Key Laboratory of Natural Resources Spatial Information, Handan 056038, China
[4] Institute of Photogrammetry and Remote Sensing, Chinese Academy of Surveying & Mapping (CASM), Beijing 100830, China; zhaozheng@casm.ac.cn
* Correspondence: niuyufen@hebeu.edu.cn; Tel.: +86-180-4953-4082
† These authors contributed equally to this study and shared the first authorship.

Abstract: Frequent mining activities create a series of geological and environmental problems resulting in an immeasurable loss of life and property. Adopting effective technologies that monitor the surface subsidence of mining areas reliably and accurately is necessary. Targeting problems associated with conventional distributed scatterers interferometric synthetic aperture radar (DS-InSAR) technology, we propose a DS-InSAR technology integrating unmanned aerial vehicle (UAV) photogrammetry products divided into two key technical contents: generating an external reference digital elevation model (DEM) fused with UAV DEM and refining distributed scatterers candidates (DSCs) fused with an UAV digital orthophoto map (DOM). We selected two mining areas, one in Wu'an, Hebei, and the other in Inner Mongolia, with different surface cover types, mining depths, and topographies as the research area. We used Sentinel-1A SAR images covering a mine in Wu'an from 4 November 2018 to 4 March 2019 and a mining area in Inner Mongolia from 11 June 2018 to 21 October 2018 to compare and analyze the subsidence results. We also combined these results with data from their respective field observation stations to assess accuracy. We could apply DS-InSAR technology integrated with UAV photogrammetry products to the subsidence monitoring of two mining areas with different landforms and mining characteristics. Comparing with the leveling and total station, the experimental results show that the RMSE was reduced by about 2 mm in both mining areas, and accuracy for the Wu'an region improved to a higher degree than Inner Mongolia did. Furthermore, the refinement method of DS eliminated 965 and 2948 lower-quality DSCs in the two mining areas. These demonstrate that our proposed method can effectively improve the accuracy and reliability of subsidence results from two mining areas.

Keywords: InSAR; UAV DOM; mining subsidence monitoring; distributed scatterers

Citation: Zhao, J.; Yang, X.; Zhang, Z.; Niu, Y.; Zhao, Z. Mine Subsidence Monitoring Integrating DS-InSAR with UAV Photogrammetry Products: Case Studies on Hebei and Inner Mongolia. *Remote Sens.* **2023**, *15*, 4998. https://doi.org/10.3390/rs15204998

Academic Editor: Christian Bignami

Received: 30 August 2023
Revised: 5 October 2023
Accepted: 10 October 2023
Published: 17 October 2023

1. Introduction

Mining mineral resources has simultaneously brought significant economic benefits to people and a series of geological and environmental problems. The original stress equilibrium of overlying strata in the goaf is now destroyed, inevitably leading to ground surface subsidence, causing disasters that threaten people's lives and property [1,2]. Therefore, adopting effective technical methods to obtain more accurate and reliable monitoring results is necessary. The traditional mining of subsidence monitors deformation by setting up observation stations on the spot and obtaining changes in elevation values using level instruments, total stations, and GPS (global positioning system) receivers [3]. Although

these monitoring methods can obtain high-precision monitoring results, they have many drawbacks; for instance, they require extensive labor, are expensive to operate, and cannot obtain deformation values for an entire survey area. Therefore, it is difficult to meet the demand for long-term and large-scale monitoring of mining areas with them [4,5]. Interferometric synthetic aperture radar (InSAR) is a rapidly developing remote sensing technology with the advantages of wide coverage, low cost, high spatiotemporal resolution, and the ability to monitor all day under various weather conditions in recent years. It has been widely used for the deformation monitoring of various types of ground objects and surfaces [6–8]. To weaken or eliminate the influence of conventional differential InSAR (D-InSAR) via spatiotemporal decoherence and the atmospheric delay phase [9], time series InSAR was developed, including permanent scatterer InSAR (PS-InSAR), small-baseline subset InSAR (SBAS-InSAR), and distributed scatterer InSAR (DS-InSAR), which can provide more efficient and accurate monitoring of land subsidence [10,11]. DS-InSAR has a unique advantage in monitoring mining areas with fewer artificially constructed targets and more vegetation coverage because it can identify distributed target points [12,13]. Liu et al. proposed combining DS-InSAR technology with numerical analysis methods to study the stability of mountains in mining areas. Their results showed that mining activities at a certain distance from the mountains affect their stability through specific mechanisms [14]. In 2023, Li et al. [15] proposed an optimized distributed target InSAR time-series surface deformation monitoring method using a complex coherent matrix decomposition method for phase optimization. They obtained time-series surface deformation information from surrounding mining areas in Anshan City, proving this method's high reliability and its ability to achieve the high-precision, large-scale, and long-term surface deformation monitoring of open-pit mining areas. Also in 2023, Chen et al. [16] integrated DS InSAR with the PIM model and an arctangent time function to jointly obtain the surface deformation field in and around Yineng Coal Mine. Their results showed that the proposed integration strategy is helpful in improving the number of effective monitoring points and obtaining complete spatiotemporal information of the surface deformation of the working face.

The superiority of DS-InSAR technology in monitoring mining areas has attracted the attention of scholars. However, since DS-InSAR uses external reference DEMs to remove terrain phases during the deformation extraction process [17], the accuracy of external reference DEMs can affect deformation extraction accuracy. In addition, SAR data are limited to reflecting the geomorphic traits and characteristics of land surfaces based on intensity and coherence information. Mining areas' complex and ever-changing surface environments may cause less accurate DS extraction [18,19]. In other words, there are non-DS points (DSs with low accuracy) with incorrect deformation information. In recent years, UAV photogrammetry technology has been rapidly developed and favored by researchers for its ability to provide high-resolution and high-precision products such as DEM and DOM with a low-cost advantage. It has been widely applied in mining area monitoring research [20–22]. For DS-InSAR technology, high-precision UAV DEM can compensate for the lack of external reference DEM accuracy, and high-resolution UAV DOM can provide rich and clear spectral information about ground objects. These advantages can help resolve the other DS-InSAR problems mentioned above. Therefore, we propose a method that integrates UAV photogrammetry products (DEM and DOM) with DS-InSAR technology. This method is divided into two parts; (1) the UAV DEM is fused to obtain an external reference DEM with higher precision, providing a basis for accurate deformation information extraction, and (2) the UAV DOM is fused to refine DSCs and achieve high-precision DS extraction, thereby improving application capabilities in mining areas with fewer manually constructed targets and more vegetation coverage. Using the proposed method, we selected two typical mining areas with different landforms and mining characteristics for comparative analysis. In this paper, we demonstrate how this method can be applied to monitoring mining areas with different surface types, mining depths, and topographical conditions to obtain more accurate subsidence results.

2. Research Areas and Data Introduction

2.1. Overview of Research Areas

Figure 1 is a schematic diagram of the two mining area locations. The first mining area is located southeast of Wu'an City. Wu'an City is a county-level city under the jurisdiction of Handan City, Hebei Province. It is located south of Hebei Province and east of the Taihang Mountains and is one of the 58 key coal-producing counties (cities) and one of the four major iron ore-rich bases in China [23]. The territory has more than 20 kinds of minerals such as coal, iron, marble, and bauxite [24], among which coal and iron ore are the most famous with reserves of 2.3 billion tons and 562 million tons, respectively. The overall trend of the terrain is higher in the west and lower in the east, belonging to a hilly landform [25]. The jurisdiction has five fourth-order tributaries (Nanming River, Beiming River, Ming River, Mahui River, and Silt River). Figure 2 shows the land cover classification of the two mining areas, with the selection of land cover types, referencing [26]. There are many types of ground features distributed throughout the mining area, including bare land, cultivated land, artificial buildings, and shrubs, which are widely distributed and dense. The study area is based on the impact of mining on the upper part of the 132,135 working face. The strike length of the working face is 840 m, the dip length is 75 m, the average thickness of the coal seam is 5 m, the dip angle is between 21° and 25°, and the average buried depth is 550 m. The working face was pushed from north to south, and the mining method was fully mechanized top-coal caving mining for inclined longwalls. Mining was officially resumed in February 2018 and stopped in June 2019.

The second mining area is located northeast of Ejin Horo Banner, Ordos City, Inner Mongolia Autonomous Region, and south of Dongsheng Coalfield. The longitude is between 110°01′56″ and 110°01′57″, and the dimensions are between 39°38′20″ and 39°38′21″ [27]. The overall terrain in the mining area is low in the west and high in the east, with many valleys distributed on the surface, which is a typical erosive hilly and semi-desert landform [28]. The surface of the area is mostly grassland and bare land, and shrubs are distributed in patches throughout the area, with few artificial buildings (Figure 2b). We examined the impact of mining on the 2S201 working face at the upper surface of the mining area as the second research area. The strike length of the working face is 1252 m, the inclination length is 260 m, the average mining depth of the coal seam is 200 m, the average mining thickness is 3.3 m, and the average inclination angle is 2°. Mining was pushed from south to north, starting in mid-July 2018 and being completed in late October 2018 for a total of 105 days.

We compared the similarities and differences between the two mining areas in terms of land cover types. Shrubs are widely distributed in the two mining areas; they are gathered in piles in the Wu'an mining area but are messy and scattered in the Inner Mongolia mining area. In addition, there are more houses in the Wu'an mining area than in the Inner Mongolia mining area. In terms of coal seam depth, the average depth of coal seams buried in the Wu'an mining area is 550 m, whereas the average mining depth in the Inner Mongolia mining area is 200 m. In terms of terrain, a river runs through the Wu'an mining area, with a relatively flat terrain that is low in the middle and slightly higher in the north and south. The Inner Mongolia mining area is crisscrossed by valleys with steep terrain high in the east and low in the west. Both mining areas have different typical characteristics that test the proposed method's applicability, reliability, and accuracy in determining subsidence results.

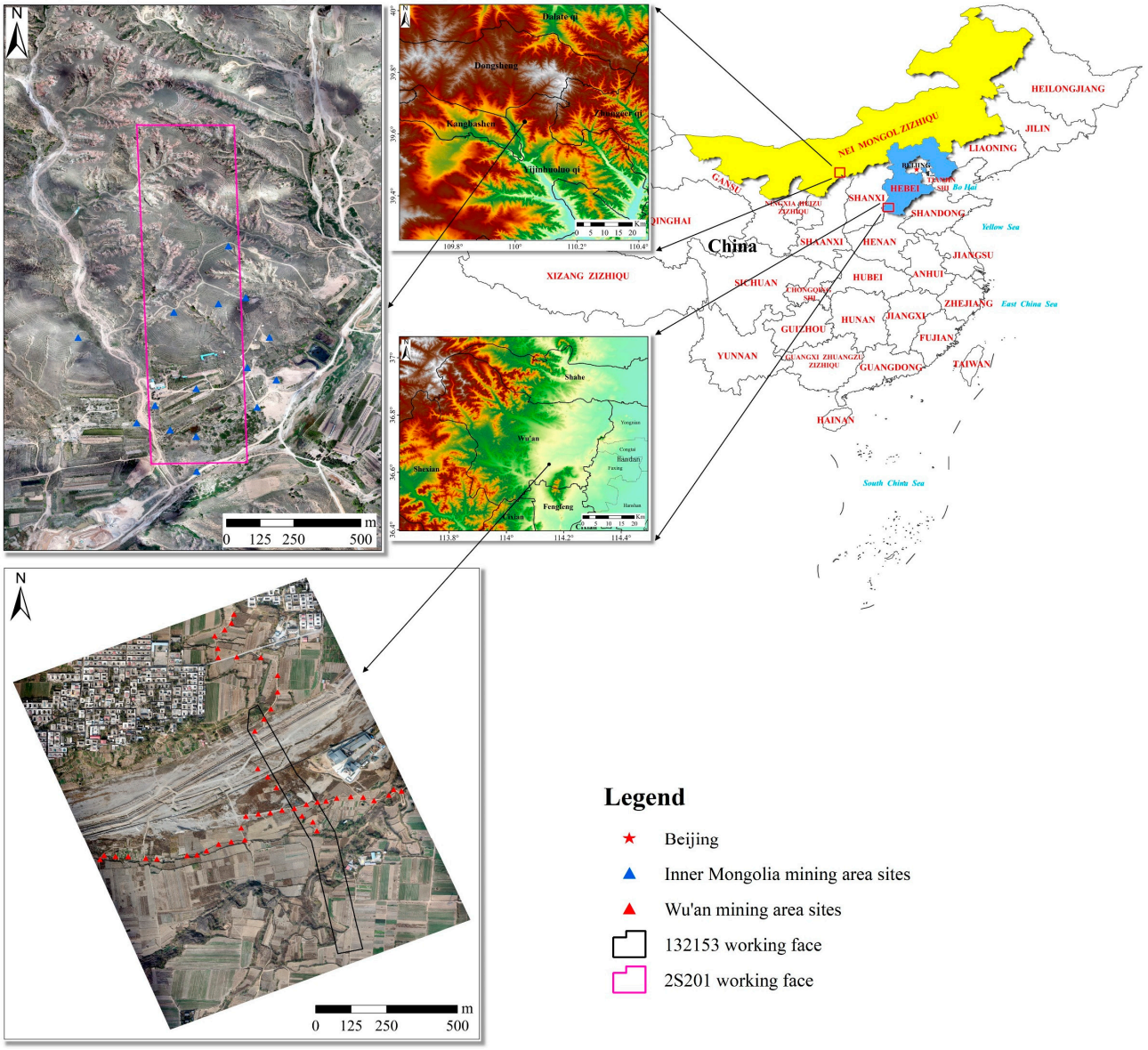

Figure 1. Schematic diagram of the two study area locations.

2.2. *Introduction of Data Set*

2.2.1. SAR Data Sets

In this study, we used single-look complex images (SLC) of the VV-polarized ascending orbit Sentinel-1A for data calculation, which can be downloaded from the official website of the European Space Agency (ESA). The image time periods selected for the two mining areas were 4 November 2018–4 March 2019 in Wu'an City and 11 June 2018–21 October 2018 in Inner Mongolia. Table 1 shows the dataset parameters used in the two mining areas.

Table 1. Parameters of the SAR data sets in two mining areas.

Region	Sensor	Wavelength (cm)	Numbers	Orbit Directions	Start Date	End Date
Wu'an	Sentinel-1A	5.56	11	Ascending	4 November 2018	4 March 2019
Inner Mongolia	Sentinel-1A	5.56	12	Ascending	11 June 2018	21 October 2018

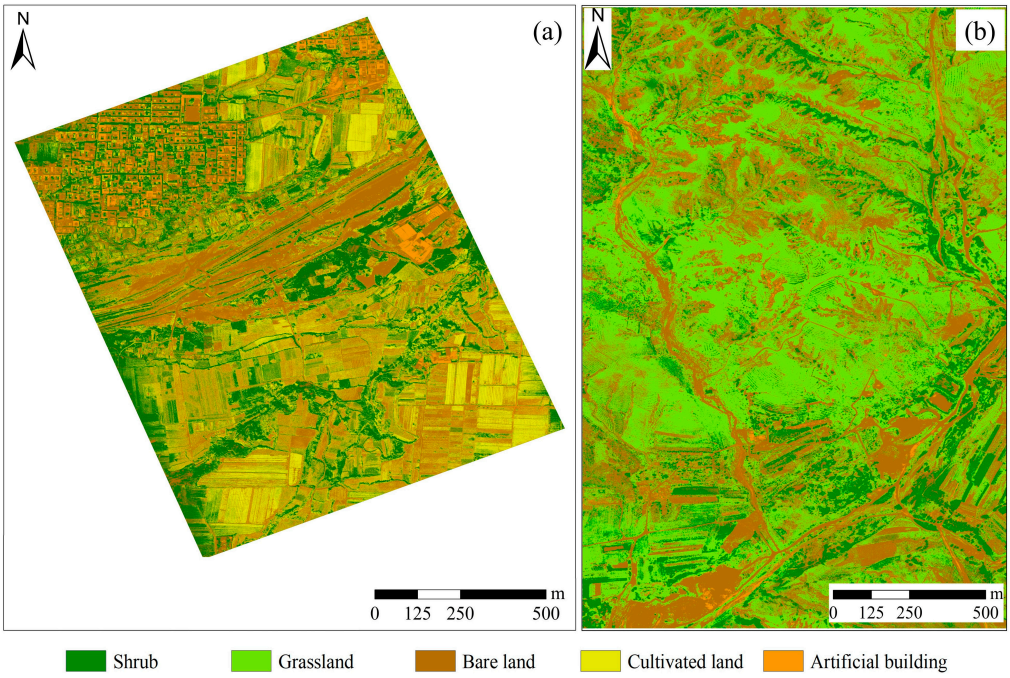

Figure 2. Land cover types of mines in Wu'an, Hebei (**a**), and Inner Mongolia (**b**).

2.2.2. UAV Photography

The UAV photography in Wu'an used the Trimble UX5 drone aerial survey system equipped with a charge-coupled-device (CCD) camera to collect images on-site. Based on the terrain conditions on the surface of the 132,153 working face and the endurance time of the drone, the route height was determined to be 150 m, and the forward overlap and side overlap are 80%. The collection time was 28 April 2018 (Table 2). The UAV photography of a mining area in Inner Mongolia also involved using the Trimble UX5 drone aerial survey system, but equipped with a SONY A5100 SLR camera to collect images on site. Based on the terrain above the 2S201 working face and the height of the surrounding high-voltage line towers, the route height was set to 230 m, and the forward overlap and side overlap were 80%. The collection time was 9 June 2018. The UAV DEMs generated in both mining areas have a resolution of 4 m (Table 2).

Table 2. Parameters for UAV photography collection.

Region	UAV	Camera	Forward Overlap (%)	Side Overlap (%)	Flight Altitude	Acquisition Date
Wu'an	Trimble UX5	CCD	80	80	150	28 April 2018
Inner Mongolia	Trimble UX5	SONY A5100	80	80	230	9 June 2018

The UAV DEM was obtained after the UAV photographs were processed via aerial triangulation to generate point clouds. Then, they were processed via filtering, denoising, extracting ground points, and interpolation [29,30]. The resolution of UAV DOM is 0.5 m, which was also processed from UAV photography photos.

2.2.3. Other Data Sets

Shuttle radar topography mission DEM (SRTM DEM) data were obtained from the United States Geological Survey (USGS) website with a 30 m resolution [31] for InSAR processing.

In addition, field observation station data were obtained to test the accuracy of monitoring results for the two mining areas. The leveling observation data (Figure 1) for the Wu'an mining area include two phases, 31 October 2018 and 1 March 2019, which were

obtained by observing the direction and inclination of the working face. The total station observation data (Figure 1) for the Inner Mongolia mining area also include two phases, 9 June 2018 and 16 October 2018, which were obtained from stations distributed within the mining area. Figure 1 shows the locations of field observation stations in the two mining areas.

2.2.4. Related Software and Codes

GAMMA software was used for InSAR processing, such as generating interferograms and geocoding. Jiang's open-source program package DSIpro was used for DS-InSAR processing [32]. And the maps were constructed with version 10.3 of ArcGIS software.

3. Research Methods

In this study, we used DS-InSAR technology integrated with UAV photogrammetry products to simultaneously process SAR image datasets covering two mining areas in Wu'an and Inner Mongolia. The main technical process (Figure 3) is divided into obtaining fused external reference DEMs; DS-InSAR data processing and accuracy comparison based on fused DEMs; and DSC refinement and verification fused with UAV DOM.

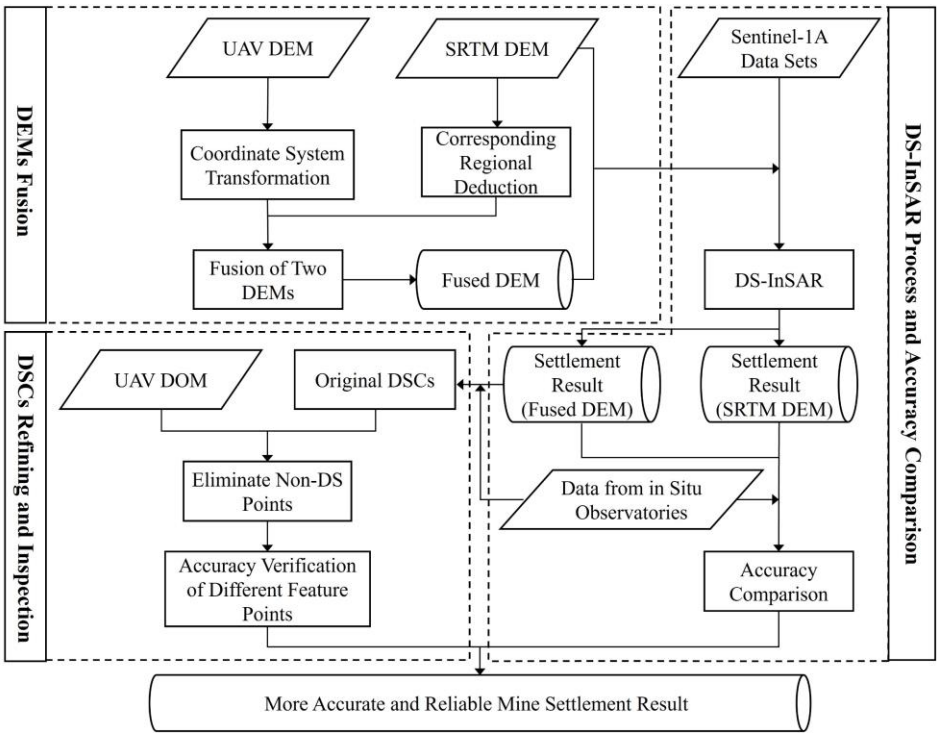

Figure 3. Technical flow chart of this research.

3.1. Generation of InSAR Reference DEM Fused with UAV DEM

We integrated UAV DEMs from local mining areas with large-scale SRTM DEMs, and used the resulting fused DEMs as external reference DEMs to participate in InSAR data processing. This not only could improve the accuracy of InSAR calculation in local mining areas, but also could greatly save costs. However, due to the inconsistency of the coordinate systems (plane and elevation) between the two DEMs, we needed to use one DEM as a reference and then perform coordinate system conversion on the other DEM.

The specific steps of fusion are as follows: (1) based on the SRTM DEMs, the UAV DEM plane coordinate system is converted using a four-parameter method; (2) based on SRTM DEMs, the elevation correction of UAV DEMs is conducted by obtaining the average elevation difference from common sample points; (3) to avoid damaging the original elevation value of the UAV DEM, the SRTM DEM part corresponding to the UAV DEM is

removed; (4) the processed UAV DEM and SRTM DEM are fused via chimera fusion, which produces a fused DEM used as the external reference DEM.

3.2. DS-InSAR Integrated with UAV DOM

3.2.1. Selection of DSs

Depending on whether or not there are dominant sub-scatterers in the SAR image resolution unit, ground targets can be divided into permanent and distributed scatterers [33]. The scattering characteristics of DSs are moderate, meaning that there is no backscattering signal from any ground object in the pixel occupying the dominant position of the pixel signal. Common examples in nature include bare land, dirt roads, deserts, and grasslands [34–36]. DS extraction from conventional DS-InSAR requires statistical testing based on amplitude or intensity images in the time dimension to determine statistically homogeneous pixels (SHPs) for each pixel. Then, the pixel phase is optimized based on the homogeneity of the target pixel. Finally, the phase optimization quality is evaluated, and the number of homogeneous pixels and temporal coherence thresholds is set to filter out DSs with better coherence and a higher signal-to-noise ratio [37,38]. However, the DS selection of conventional DS-InSAR could negatively impact the accuracy of DS extraction; therefore, some non-DS points were also selected as DSs. We propose a DS selection method that integrates UAV DOM. Based on conventional DS selection, non-DS points can be eliminated based on the high-resolution UAV DOM, which contains rich ground coverage information. The specific steps are as follows: (1) the type of ground coverage on the UAV DOM is determined via visual interpretation; (2) by manually selecting training samples, the maximum likelihood method is used to extract the distribution area of ground objects corresponding to non-DS points on the UAV DOM; (3) the surface object distribution areas of non-DS points through manual visual interpretation are selected; (4) the surface object distribution areas of non-DS points are superimposed with the original DSCs to eliminate non-DS points.

3.2.2. DS-InSAR Principle and Process

The principle of DS-InSAR is to compare the similarity between interferogram time dimension samples, select pixels with statistically similar scattering characteristics for homogeneous filtering, and optimize their phase estimation in the complex domain. These steps can effectively improve the quality of the interferometric phase and the accuracy of time series displacement estimation for each point target [39]. Compared with other time-series InSAR, DS-InSAR adds two steps of homogeneous pixel identification and phase optimization [40], which resolve the problem of insufficient target points and uneven distribution in low-to-medium coherence areas. The DS-InSAR processing flow of this paper is as follows.

(1) Considering the mining subsidence characteristics, we adopted a multi-primary image strategy to construct a differential interferogram and use the fused DEM as an external reference DEM to participate in removing the terrain phase. (2) Based on the amplitude information of SAR images, we adopted the fast statistically homogeneous pixel selection (FaSHPS) algorithm to identify SHPs and set a threshold for the number of homogeneous pixels according to different mining areas. Pixels above the threshold were used as preliminary DSCs. (3) We optimized the phases of the preliminary DSCs, and evaluated the quality of the optimized phases by taking the fit (also known as temporal coherence) between the phases before and after optimization as the evaluation index, taking the pixels above the set temporal coherence threshold as the original DSCs. (4) We used the minimum cost flow (MCF) method to unwrap the phase of the original DSCs while removing the atmospheric delay phase. (5) We established an observation equation for the phase change rate and unwrapped phase and used the singular-value decomposition (SVD) method to solve the generalized least squares solution of the equation. (6) After obtaining the deformation results of the original DSCs through phase-to-vertical deformation and

anti-geocoding, we combined them with high-resolution UAV DOM to eliminate existing non-DS points; in this way, we obtained the deformation results for the refined DSCs.

The temporal coherence calculation formula for DSs [41] is

$$\gamma_{DS} = \frac{1}{N(N-1)} \sum_{N}^{n=1} \sum_{N}^{m=n+1} \exp^{i(\phi_{mn} - (\phi_m - \phi_n))} \quad (1)$$

where γ_{DS} is the temporal coherence; ϕ_{mn} is the interferometric phase before phase optimization; ϕ_m and ϕ_n are the respective phases after phase optimization; and N is the number of SAR images.

3.3. Accuracy Evaluation

We set up on-site observation stations for the direction and inclination of the working face in the Wu'an mining area and conducted periodic observations of these stations using level instruments. Similarly, we evenly arranged field observation stations in and around the center of the working face in the Inner Mongolia mining area. According to terrain conditions, we used the total station to observe stations periodically. The field observation data of the two mining areas were regarded as true values.

Combined with the field observation data of the two mining areas, two kinds of accuracy evaluations were conducted; (1) based on the DS-InSAR subsidence results obtained using the fused DEM and the original DEM (SRTM DEM) as the external reference DEM, we extracted the InSAR monitoring values of the corresponding field observation stations; furthermore, accuracy comparisons and quantitative analyses were conducted combined with field observation data; (2) to verify whether or not non-DS surface object types lead to low monitoring accuracy, we used UAV DOM to classify surface object types corresponding to field observation stations. Then, based on the subsidence results of DS-InSAR before the refinement of DSCs, we extracted the InSAR monitoring values of corresponding field observation stations according to ground object types and compared the InSAR monitoring values of different ground object types to data from field observation stations.

4. Results

4.1. The Fused DEM

The UAV DEMs of the two mining areas were inconsistent with the SRTM DEM coordinate system. The horizontal and vertical datum of the UAV DEM in Wu'an City mining area were the Xi'an Geodetic Coordinate System 1980 and National Height Datum 1985, respectively. The UAV DEMs in the Inner Mongolia mining area were the Beijing Geodetic Coordinate System 1954 and the Yellow Sea Height Datum 1956, respectively. The SRTM DEMs were WGS84 and Earth Gravitational Model 1996 (EGM96) [42]. We used the four-parameter method of common point calculation and elevation correction to convert the plane and elevation of the two DEM types.

When using elevation correction to convert the elevation system, the elevation value of the UAV DEM of the Wu'an mining area was bound to change due to the mining impact of the corresponding working face. The UAV photographs of the Wu'an mining area were collected on 28 April 2018 and mining started on the corresponding 132,153 working face in February 2018. To ensure the reliability of elevation correction, we evenly distributed sample points from the four corners of the UAV DEM in the Wu'an mining area far from the mining range of the working face, as shown via the black triangle in Figure 4a. The UAV DEM of the Inner Mongolia mining area would not be affected by the mining of the working face. Therefore, we uniformly arranged sample points throughout the entire range, as shown by the black triangles in Figure 4b.

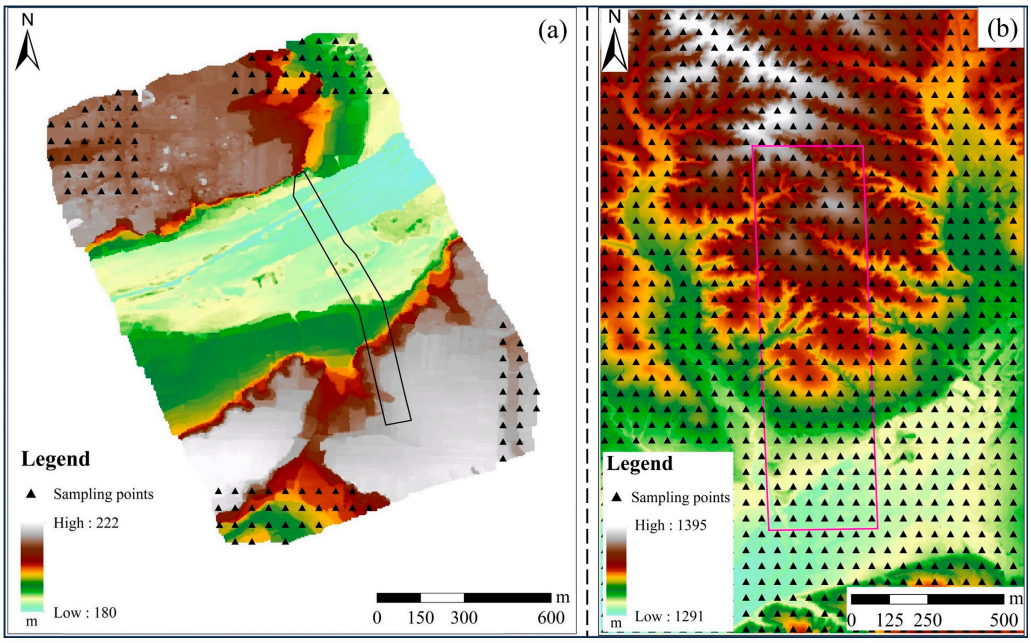

Figure 4. Layout of sample points in two mining areas. (**a**) Wu'an mining area; (**b**) Inner Mongolia mining area.

We extracted the elevation values of SRTM DEM and UAV DEM for the sample points of the two mining areas separately and calculated the average elevation difference for both. The average obtained can be regarded as the difference between the UAV DEM and the SRTM DEM elevation data. Since the UAV DEM elevation values in both mining areas are relatively small compared to the SRTM DEM elevation values, elevation correction can be achieved by simply adding the average height difference values obtained from each area to the UAV DEM of the corresponding mining area. After extracting the corresponding UAV DEM areas from the SRTM DEM of the two mining areas, the UAV DEM and SRTM DEM were fused by mosaicking. Figure 5 shows the fused DEMs obtained from the two mining areas. Figure 5a shows the fused DEM of the Wu'an mining area, and Figure 5b shows the fused DEM of the Inner Mongolia mining area. A distance of 20 m was used to generate the contour lines of the fused DEMs, and they are smooth without truncation, indicating that the two mining areas' DEM fusion effects were well integrated.

4.2. DS-InSAR Results Based on Fused DEMs

After obtaining the fused DEMs from the Wu'an and Inner Mongolia mining areas, we used each fused DEM as the external reference DEM and selected SAR images from their respective time periods. After DS-InSAR data processing, we obtained subsidence monitoring results for both mining areas (Figure 6). Figure 6a,b is the DS-InSAR subsidence results for the Wu'an and Inner Mongolia mining areas obtained using the fused DEM as the external DEM.

The parameters set in the data processing process for the two mining areas underwent repeated experiments. For the Wu'an mining area, we set the maximum time and space baselines to 60 d and 150 m, the date of the selected reference main image was 3 January 2019, the set threshold for the number of homogeneous points was 75, and the threshold for temporal coherence was 0.6. For the Inner Mongolia mining area, we set the maximum time and space baselines to 15 d and 150 m, the selected reference main image date was 10 August 2018, the set threshold for the number of homogeneous points was 35, and the threshold for temporal coherence was 0.45.

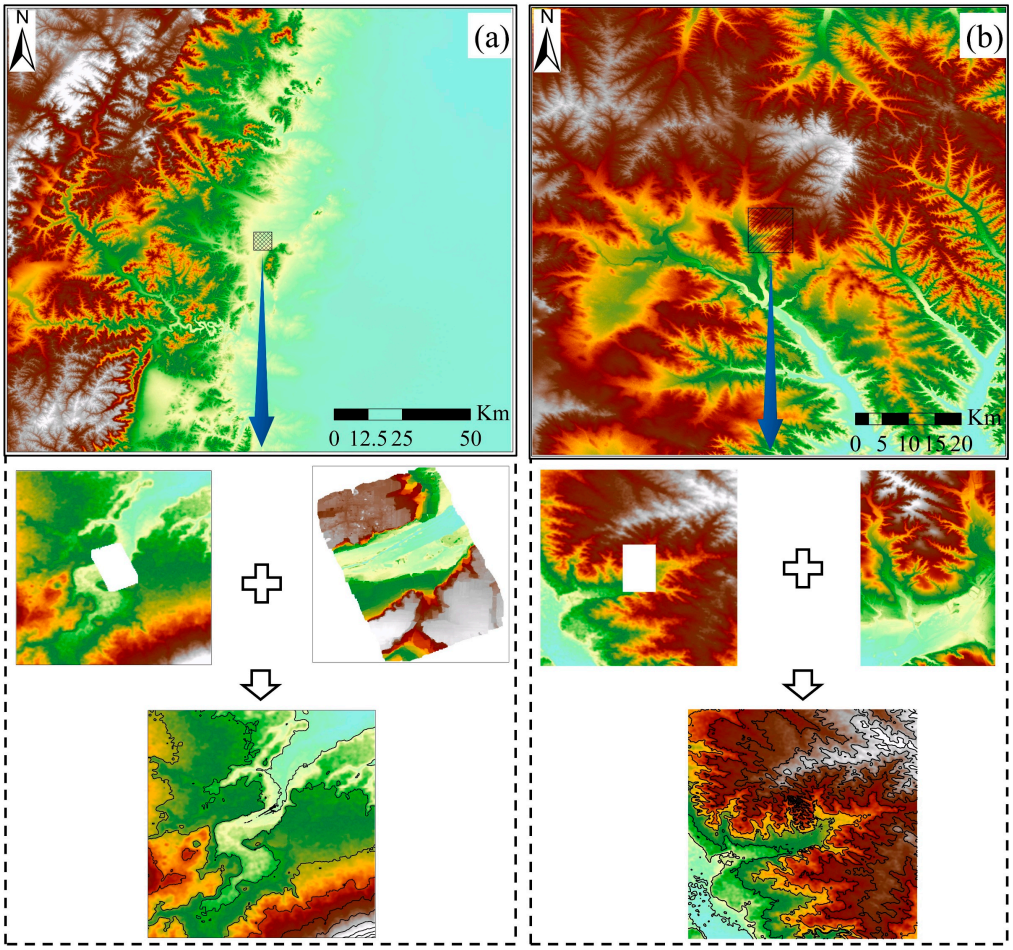

Figure 5. Schematic diagram of DEM fusion. (**a**) Wu'an mining area; (**b**) Inner Mongolia mining area.

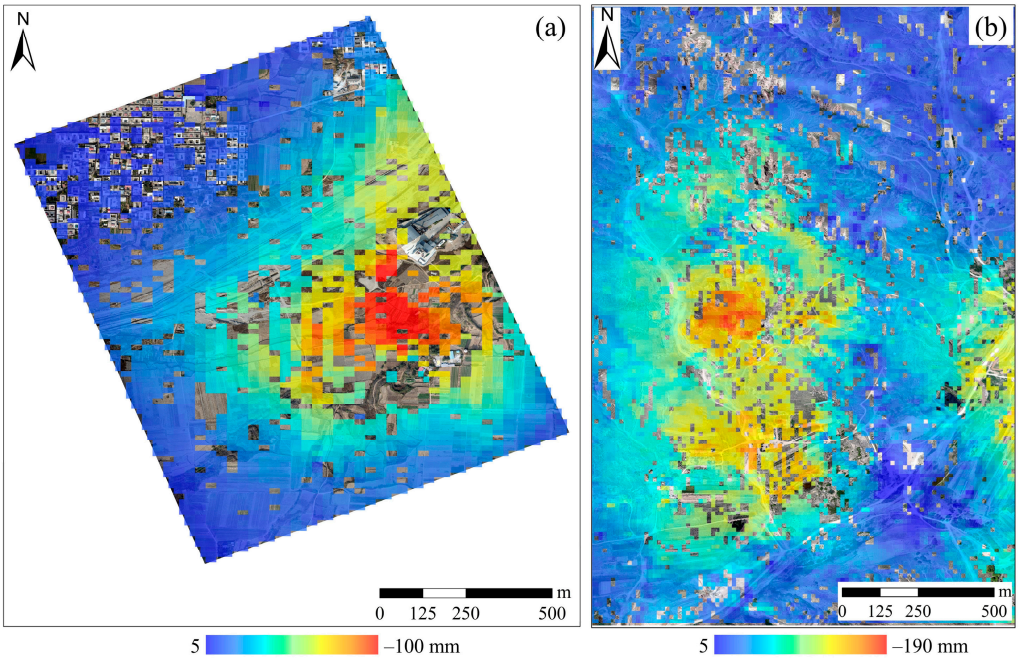

Figure 6. DS-InSAR subsidence results based on the fused DEMs of the Wu'an (**a**) and Inner Mongolia mining areas (**b**).

4.3. Refinement of DSCs

Some non-DS points or inaccurate DSs appeared in the DS-InSAR subsidence results mentioned in the previous section, which affected the accuracy of the results. After integrating high-resolution true-color UAV DOM, we discovered that the ground types of non-DS points in the two mining areas were shrubs through visual interpretation. Therefore, extracting the distribution area of shrubs was the first step to eliminating non-DS points. Firstly, we manually selected training samples from the UAV DOMs of the two mining areas. We used the maximum likelihood method to extract the shrub distribution area from the DOM. Then, according to the distribution characteristics of shrubs, the patch area was used as the evaluation standard, and the Wu'an mining area was set a threshold of 100 m^2 to remove fragmented patches, while the Inner Mongolia mining area was set a threshold of 0.25 m^2 to remove smaller, messy patches. To select more shrub distribution areas from the two mining areas, we combined their true color DOMs and eliminated the misidentified patches through visual interpretation. The final extraction effect is shown in Figure 7. The color red indicates the shrub distribution area, which is consistent with the corresponding DOM image.

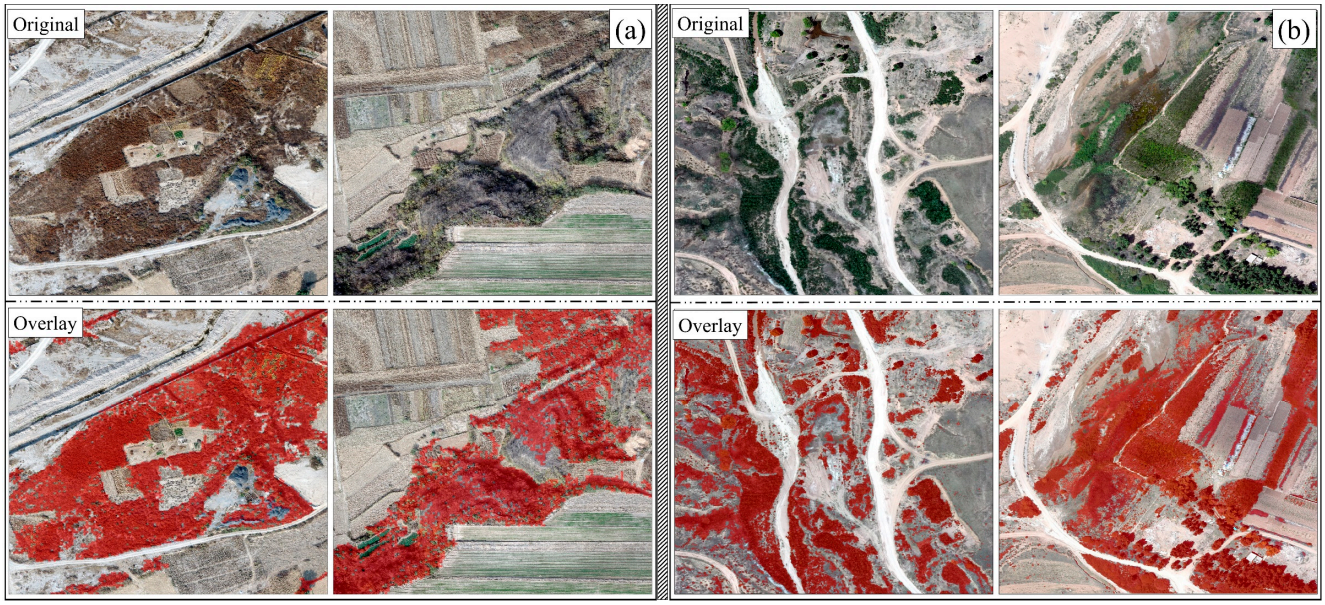

Figure 7. Shrub extraction areas before (above) and after (below) stacking in the Wu'an (**a**) and Inner Mongolia mining areas (**b**).

We superimposed the extracted shrub distribution area onto the original DSCs to eliminate non-DS points, as shown in Figure 8. The number of original DSCs in the Wuan mining area was 4723, and the number after removing non-DS points was 3758. The number of original DSCs in the Inner Mongolia mining area was 12,614, and the number after removing non-DS points was 9666. Figure 9 shows the subsidence results of the two mining areas after refining the DSCs. The fused DEM was used as the external reference DEM, and non-DS points existing in the original DSCs were eliminated. Compared to the subsidence results obtained via conventional DS-InSAR, this method improved accuracy and reliability to a certain extent.

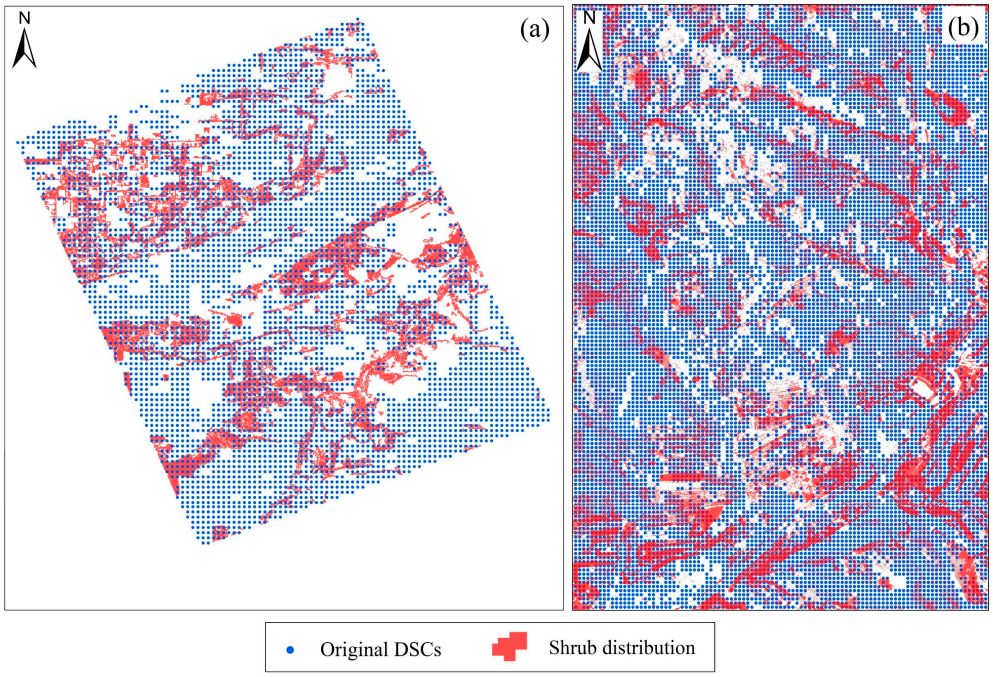

Figure 8. Distribution of original DSCs and shrubs in the Wu'an (**a**) and Inner Mongolia mining areas (**b**).

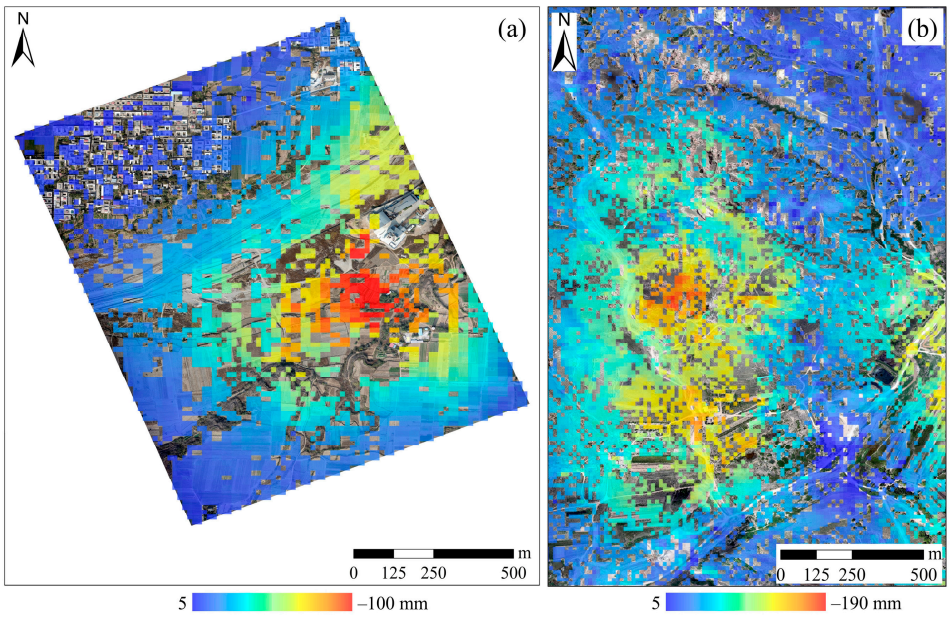

Figure 9. The refined DS-InSAR subsidence results of the Wu'an (**a**) and Inner Mongolia mining areas (**b**).

5. Analysis

5.1. Analysis of Accuracy

5.1.1. Accuracy Verification of DS-InSAR Results Based on the Fused DEM

To test whether or not the accuracy of the DS-InSAR monitoring results obtained using a fusion DEM as the external DEM improved, we used the original DEM as the external reference DEM. After processing with DS-InSAR, we obtained the monitoring results of the two mining areas. The parameters set in the two mining areas were consistent with those set when the fused DEM was used as an external reference DEM. Combined with the data from the field observation stations in the two mining areas, we compared the accuracy of

the monitoring results for each mining area based on the original and fused DEMs in a line graph (Figure 10).

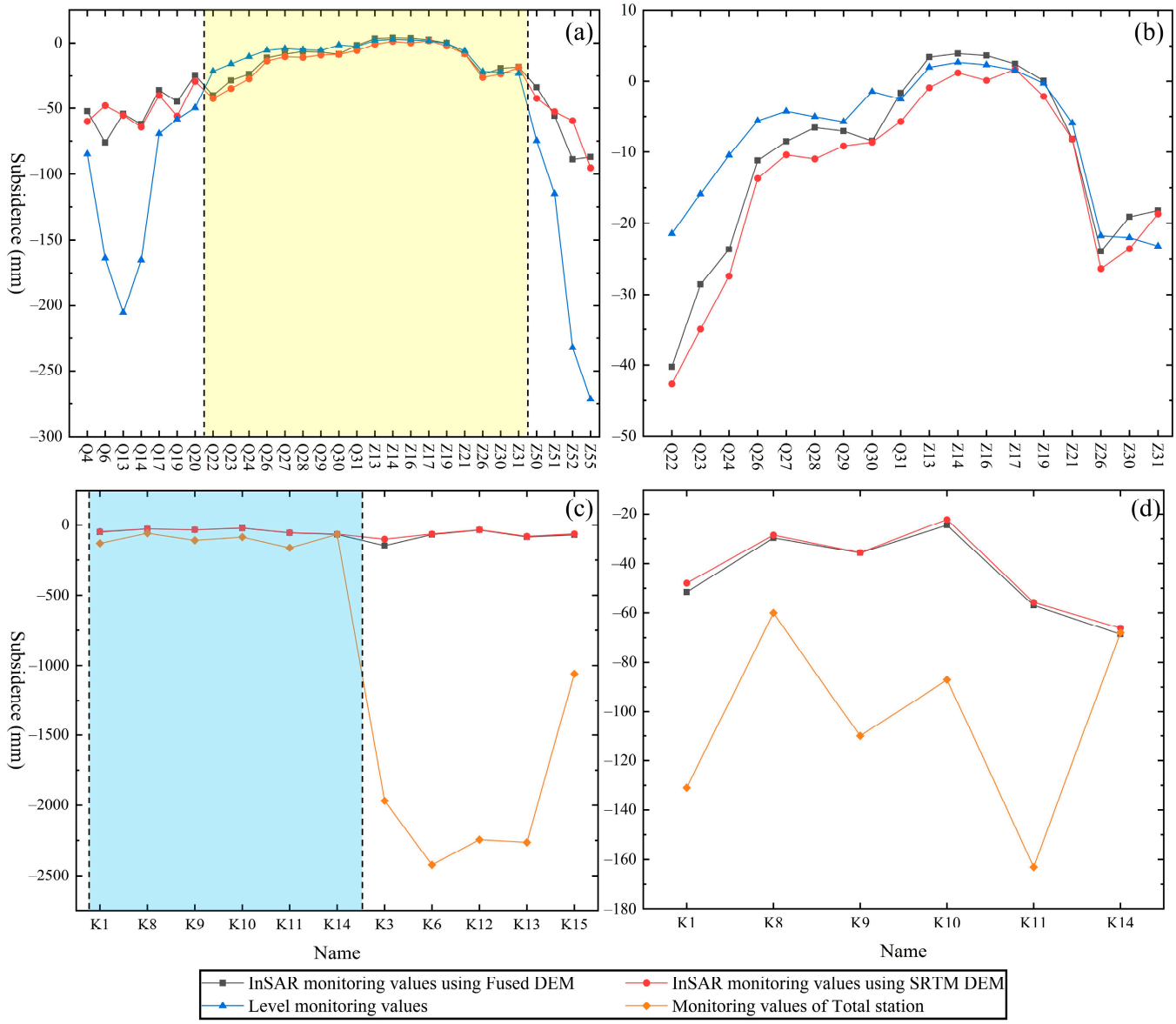

Figure 10. Accuracy comparison between monitoring values in the two mining areas. (**a**) Accuracy comparison in Wu'an mining area; (**b**) the detail display of the yellow area in (**a**); (**c**) accuracy comparison in Inner Mongolia mining area; (**d**) the detail display of the blue area in (**c**).

Figure 10a,b compares the accuracy of monitoring results in the Wu'an mining area. In Figure 10a, the monitoring values in the yellow area show good deformation variables and trends (as shown in Figure 10b), whereas monitoring values at points outside the yellow area show significant differences. When actual surface deformation variables exceed the range that InSAR can monitor, unwrapping errors occur, resulting in incorrect deformation information [43,44]. Figure 10c compares the accuracy of monitoring results in the Inner Mongolia mining area. The InSAR monitoring values for points in the blue area are relatively close to the total station observation values (as shown in Figure 10d). The difference between InSAR monitoring values for points outside the blue area and the total station observation values reach the meter level. For the same reasons, unwrapping errors occur when deformation levels exceed InSAR's monitoring range. In Figure 10d, the difference between InSAR monitoring values and total station observation values for each point increases with the increase in real deformation. The difference at the K14 point is relatively

small, whereas at K8 and K14, the deformation levels are similar but significantly different. Combined with high-resolution DOM, we found that the ground type corresponding to K14 is thin grassland, while the ground type at K8 is shrub (Figure 11b). By observing Figure 10b,d, we found that the InSAR monitoring value obtained using the fused DEM as the external reference DEM is closer to the field observation value than the that obtained when using original DEM.

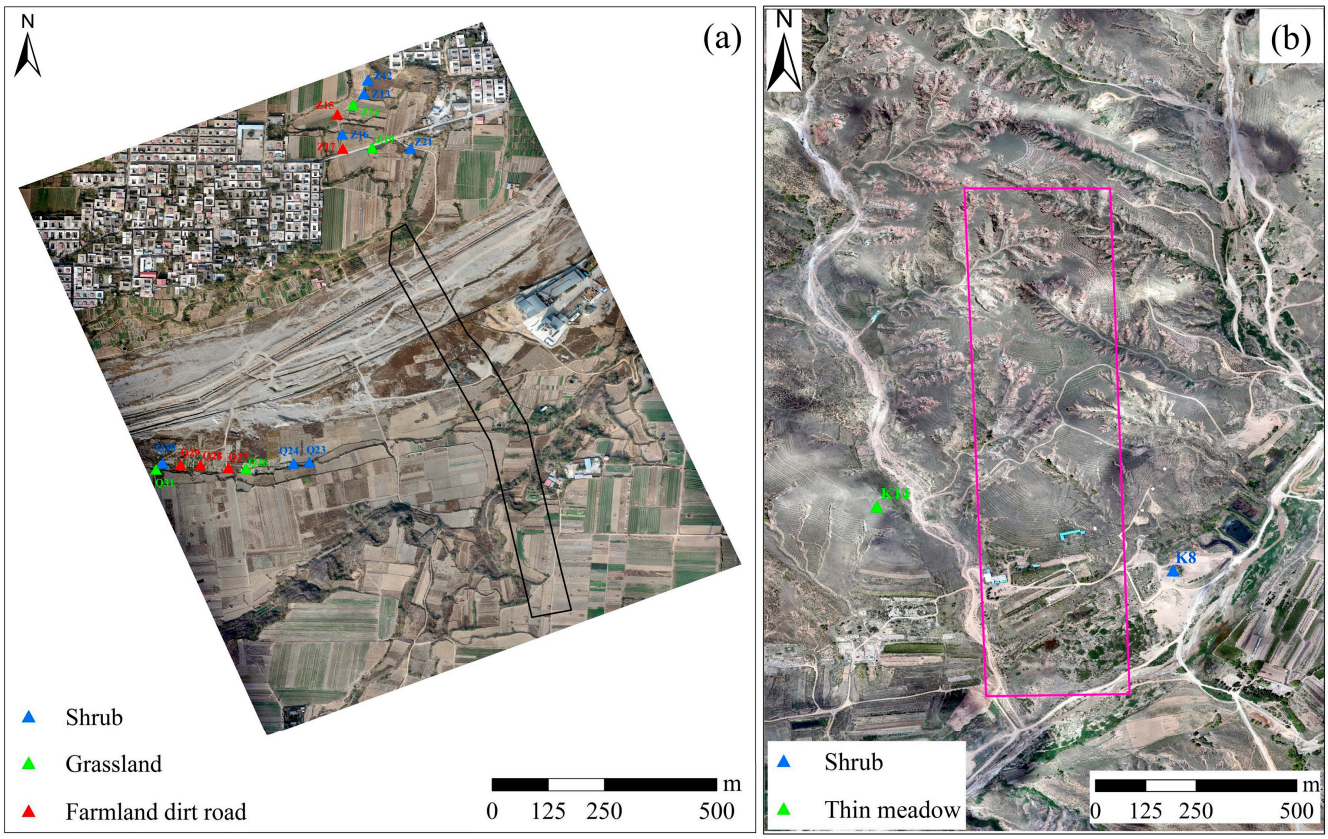

Figure 11. Classification maps of Wu'an (**a**) and Inner Mongolia mining areas (**b**).

To quantify differences in accuracy between the two InSAR monitoring results, we extracted differences from the two InSAR monitoring values in Figure 10b,d and their respective field observation station data and counted two different types of errors, as shown in Table 3. The statistical error results of the two mining areas show that the two error types when using the fused DEM as an external DEM are lower than those when using the original DEM as an external DEM. The monitoring accuracy of the Wu'an mining area increased by 2 mm, and that of the Inner Mongolia mining area also increased by 2 mm.

Table 3. Accuracy comparison between two InSAR deformation results in the Wu'an and Inner Mongolia mining areas.

Type of Error	Wu'an		Inner Mongolia	
	SRTM DEM	Fused DEM	SRTM DEM	Fused DEM
RMSE (mm)	8.8	6.8	69.7	68.2
MAE (mm)	6.3	4.6	60.5	58.8

In Table 3, the InSAR monitoring errors of the Inner Mongolia mining area are relatively large, whereas those of the Wu'an mining area are much smaller. These findings are so

because the actual deformation gradient of the Inner Mongolia mining area is relatively large, and the main factors affecting actual deformation are the mining depth and thickness of the coal seam. The average buried depth of the coal seam in the Wu'an mining area is 550 m, and the average thickness is 5 m. The average buried depth of the coal seam in the Inner Mongolia mining area is 200 m, and the average thickness is 3.3 m. The mining depth is the main reason for the large deformation gradient in the Inner Mongolia mining area. The shallower the mining depth, the greater the actual deformation caused, and vice versa. Despite this, the accuracy of the monitoring results for the Inner Mongolia mining area using the fused DEM as an external DEM showed improvement. Therefore, DS-InSAR technology using fused DEM as an external DEM can monitor mining areas with different mining depths and reduce monitoring errors.

5.1.2. Accuracy Comparison between Different Ground Object Points

To verify that non-DS points corresponding to land cover types (shrubs in this paper) could affect monitoring accuracy, we compared the monitoring accuracy of different land cover type points using field observation station data from each mining area. We visually interpreted the high-resolution UAV DOM of the two mining areas and extracted three types of ground features from the Wu'an mining area. We used the points in Figure 10b, namely shrubs, grassland, farmland with dirt roads, and ground features, including seven points for shrubs, five points for grassland, and four points for farmland with dirt roads. We also used the K8 and K14 points in Figure 10d and extracted two ground features, namely shrubs and thin grassland (Figure 11).

Combined with points from the Wu'an mining area (Figure 11a), the two error types from 4 November 2018 to 4 March 2019 were counted, as shown in Table 4. The two error types in the table follow the same rule and are arranged in descending order: shrub, grassland, and farmland with dirt roads. The target point in the shrub had the lowest monitoring accuracy and the largest error. For the two points in the Inner Mongolia mining area (Figure 11b), the terrain type of point K14 is thin grassland, with minor errors, whereas the ground type of point K18 is shrub, with relatively large errors and low monitoring accuracy. We found that ground object types (shrubs) corresponding to non-DS points cause low-precision monitoring.

Table 4. Monitoring accuracy between points of different ground object types in the Wu'an mining area from 4 November 2018 to 4 March 2019.

Type of Error	Ground Object Type		
	Shrub	**Grassland**	**Farmland with Dirt Roads**
RMSE (mm)	3.5	2.9	2.4
MAE (mm)	2.8	2.2	2.0

5.2. Advantage Analysis of DS Selection Integrated with UAV DOM

To illustrate the advantages of our point selection method over traditional coherence threshold point selection and conventional DS selection, we compared the differences in quantity and distribution between the original coherence points, original DSCs, and refined DSCs in the two mining areas. Figure 12 is a distribution map of the original coherence points in the two mining areas. The interval of coherence is [0, 1]. The better the coherence, the closer the value is to 1. Figure 12 shows that the highest coherence points in the Wu'an and Inner Mongolia mining areas are sparse, with uneven distribution characteristics. In particular, the coherence points on and near the working faces of each mining area are few and far between. In addition to the natural surface of the mining area being covered more with fewer strong scatterers, low coherence caused by mining at the working face can result [43] in large gradient deformation areas within and near the

working face. In addition, we compared the original coherence of the Wu'an and Inner Mongolia mining areas and counted the difference in coherence values between them (Table 5). The maximum, minimum, and average coherence values in the Wu'an mining area are higher than those in the Inner Mongolia mining area due to two reasons, one being that the housing area in Wu'an is larger than that in Inner Mongolia, and a large proportion of strong scatterers increases the maximum coherence and average coherence values, and the second being that the mining depth of the working face in Wu'an is deeper, resulting in a larger range of subsidence influence and a smaller subsidence gradient, whereas the mining depth in Inner Mongolia is shallower. In contrast, the subsidence influence range in the Inner Mongolia mining area is smaller, and the subsidence gradient is larger. The larger the subsidence gradient, the more likely it is to cause incoherence, thereby reducing the overall coherence of the Inner Mongolia mining area.

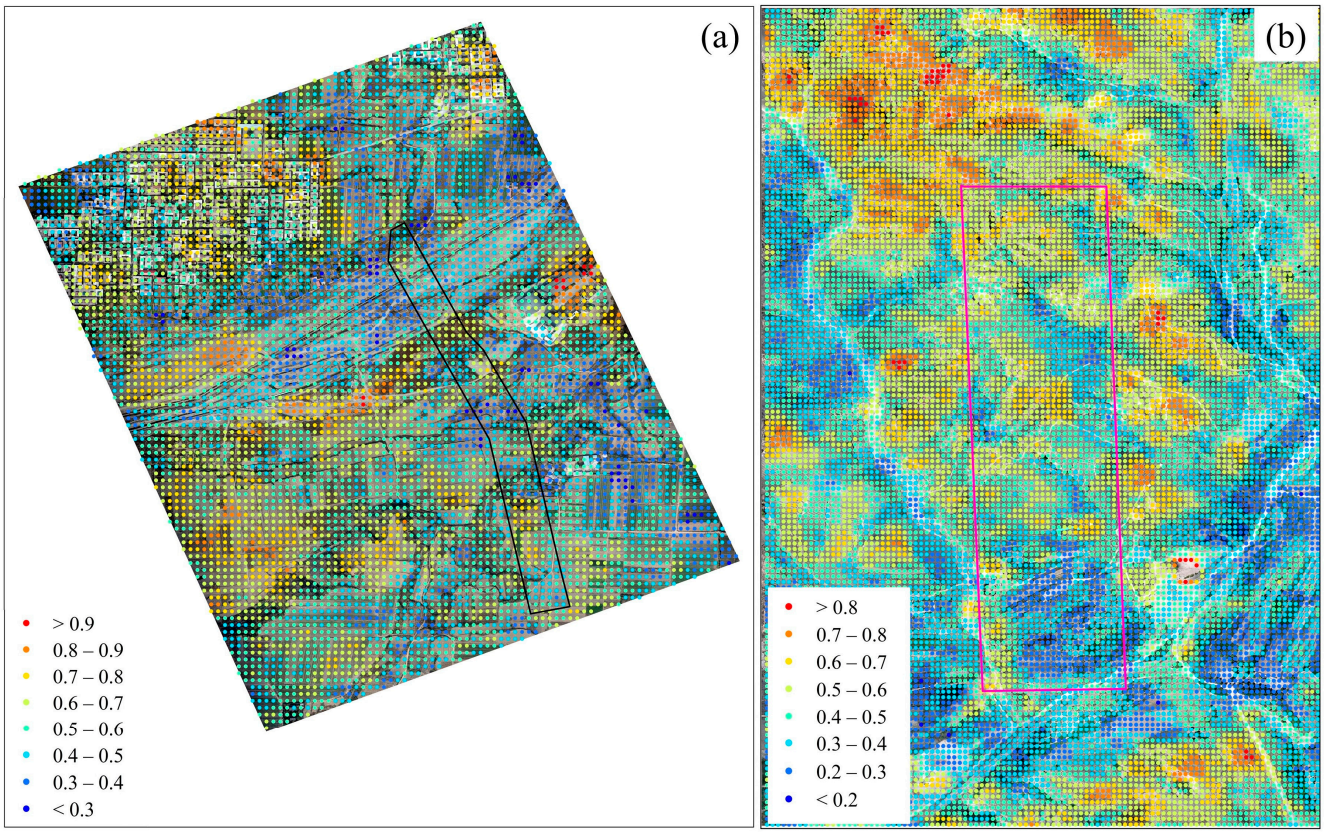

Figure 12. Distribution map of original coherent points in the Wu'an (**a**) and Inner Mongolia mining areas (**b**).

Table 5. Original coherence comparison between two mining areas.

	Wu'an	**Inner Mongolia**
Maximum	0.94	0.89
Minimum	0.25	0.19
Average	0.54	0.49

Using original coherence as a point selection index has disadvantages. Not only is there a smaller number of selected points with an uneven distribution of points but the influence of land cover type and deformation gradient causes low coherence. DS-InSAR technology uses the amplitude information of the image in the time dimension to filter out DS with moderate scattering characteristics, which reflects subsidence characteristics more comprehensively via obtaining a larger number and more evenly distributed target points, as shown in Figure 13 (blue and green dots). However, there may be non-DS points

in the DSCs selected by DS-InSAR, which are affected by the type of ground objects and lead to low-precision monitoring points. We eliminated these low-precision DSCs (green dots in Figure 13) with the help of high-precision UAV DOM and obtained refined DSCs (blue dots in Figure 13), which reflects the advantage of our point selection method. We applied this point selection method to the Wu'an and Inner Mongolia mining areas. The distribution of shrubs in the Wu'an mining area is dense and concentrated, which allows for better extraction, whereas the shrub distribution in the Inner Mongolia mining area is messy, scattered, and difficult to extract. In summary, the point selection method in this paper can be applied to mining areas with different types of land cover, but the degree of difficulty depends on the type of land cover, and its distribution.

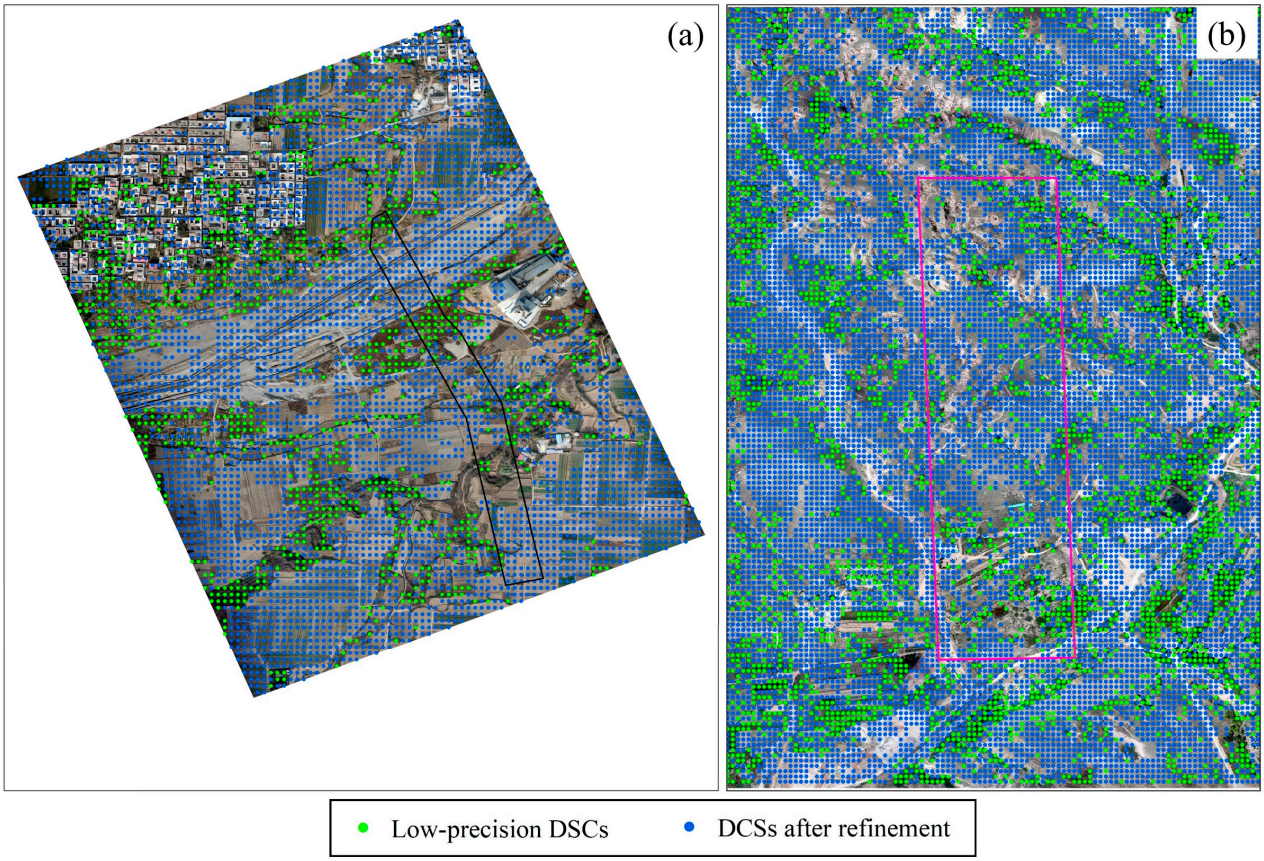

Figure 13. Low-precision and refined DSC distribution map of the Wu'an (**a**) and Inner Mongolia mining areas (**b**).

5.3. Deformation Rate Analysis of DS-InSAR Results after Refinement

We also used SBAS-InSAR technology and the fused DEM as the external DEM to process the SAR data from the two mining areas. During the data processing of the two mining areas, we used adaptive filtering methods to filter the original coherence and selected high coherence points based on the average coherence after filtering. The filtering windows for both mining areas were set to 32. After repeated experiments and comparisons, the coherence threshold for Wu'an was set to 0.9, while the coherence threshold for Inner Mongolia was set to 0.82. Figures 14a and 15a show the SBAS-InSAR processing results for the two mining areas, respectively. Figures 14b and 15b show the refined DS-InSAR results of the two mining areas using the method proposed in this paper. A comparison of the results of each mining area indicates that refined DS-InSAR can provide a more comprehensive reflection of the subsidence characteristics in the mining area than can SBAS-InSAR results. The refined DS-InSAR results can show the deformation of points within and near the working face.

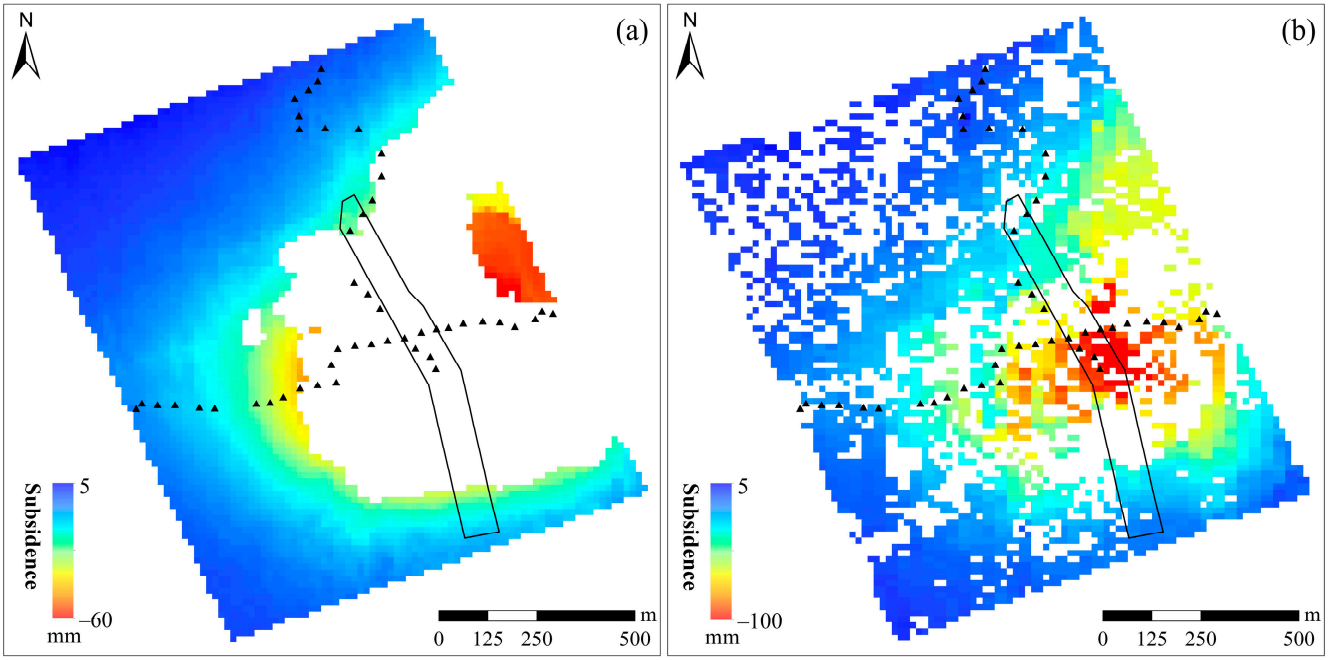

Figure 14. The SBAS-InSAR results (**a**) and refined DS-InSAR results (**b**) of the mining area in Wu'an.

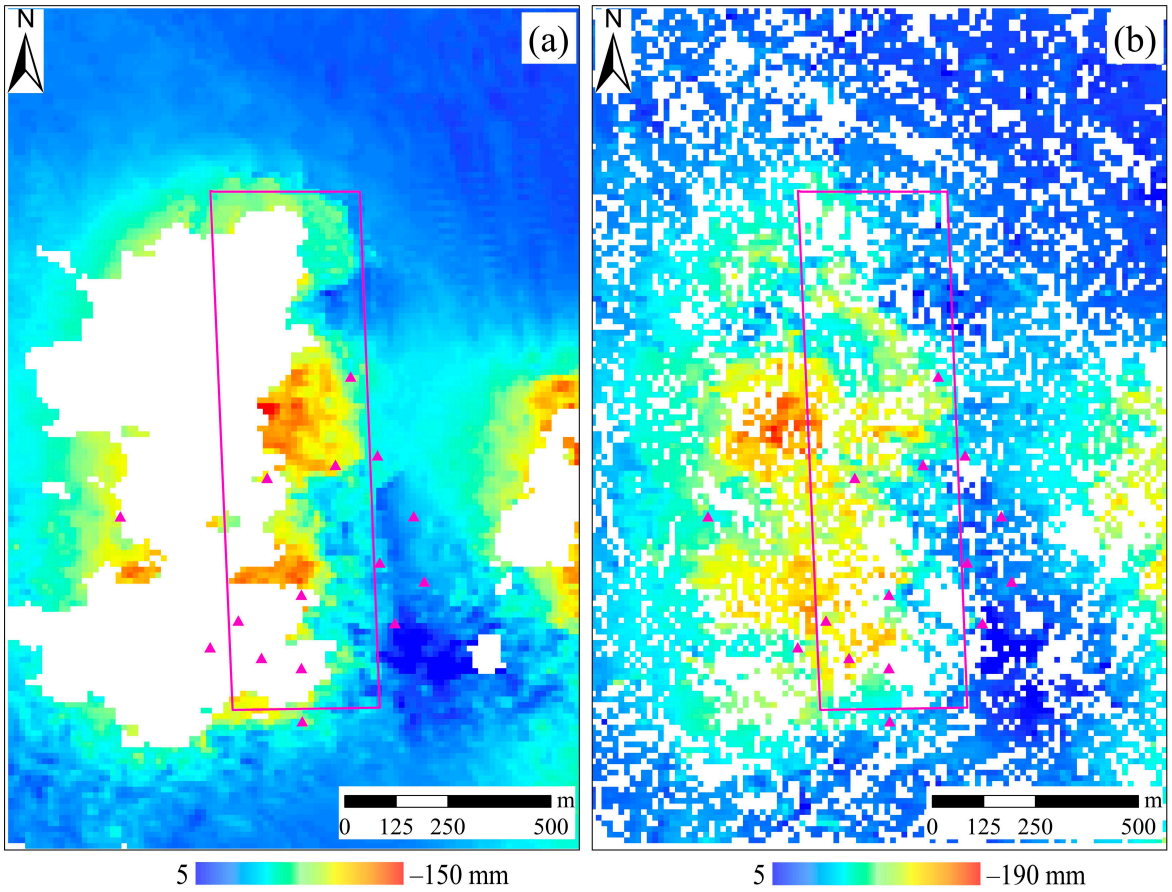

Figure 15. The SBAS-InSAR results (**a**) and the refined DS-InSAR results (**b**) of the mining area in Inner Mongolia.

Comprehensive characteristics of the mining area's subsidence allow us to analyze and understand more deformation laws in the mining area. Figures 14b and 15b show that

the mining area topography can also affect the deformation direction of the mining area. The Wu'an mining area terrain is relatively flat, and its deformation extends radially along the center of the working face to the surroundings. Deformation gradually decreases with increasing distance from the working face, which aligns with the normal law of change. In contrast, the selected mining area in Inner Mongolia has many valleys. Its terrain is high in the east and low in the west. If the influence of the small coal seam inclination is ignored, it could lead to the east side of the working face being deeper from the surface and the west side being shallower. As mentioned above, the mining depth is shallower, the deformation gradient is greater. And the converse is also true. As a result, the west side of the working face in the Inner Mongolia mining area suffers from greater deformation than the east side does.

We extracted and compared the SBAS-InSAR and refined DS-InSAR monitoring values for the corresponding locations of the field observation stations in each mining area to the data of the corresponding field observation stations, as shown in Figure 16. Figure 16a,b shows that the SBAS-InSAR monitoring values have the same deformation magnitude and trend as do the refined DS-InSAR monitoring values, and the monitoring accuracy is not significantly different. In addition to comparing the points of a few field observation stations, we also extracted common points from SBAS-InSAR, and refined DS-InSAR results of each mining area and drew them into a scatter density map (Figure 17). Figure 17a,b shows the mining areas of Wu'an and Inner Mongolia, respectively. Pearson's correlation coefficients (r) for the two mining areas are 0.96 and 0.91, respectively, suggesting that the SBAS-InSAR and refined DS-InSAR monitoring values reached a high degree of coincidence for the two mining areas. In summary, the refined DS-InSAR monitoring results could increase the number and density of target points while ensuring accuracy, thus having greater advantages over SBAS InSAR.

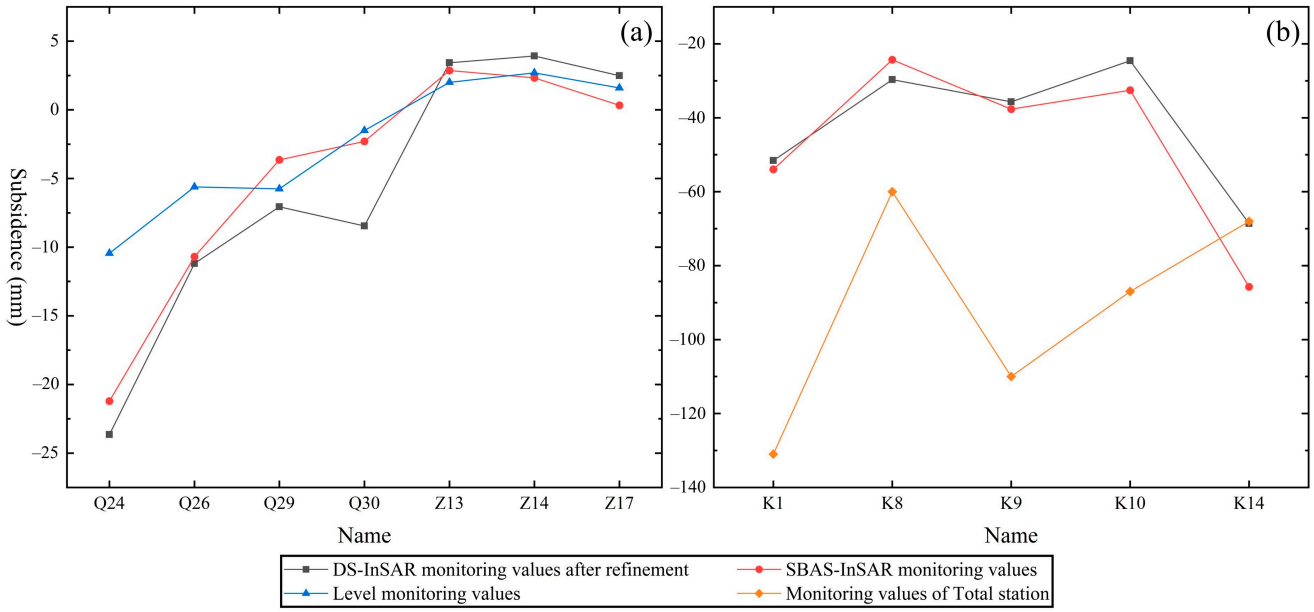

Figure 16. Comparison between SBAS-InSAR and refined DS-InSAR monitoring values in the Wu'an (**a**) and Inner Mongolia mining areas (**b**).

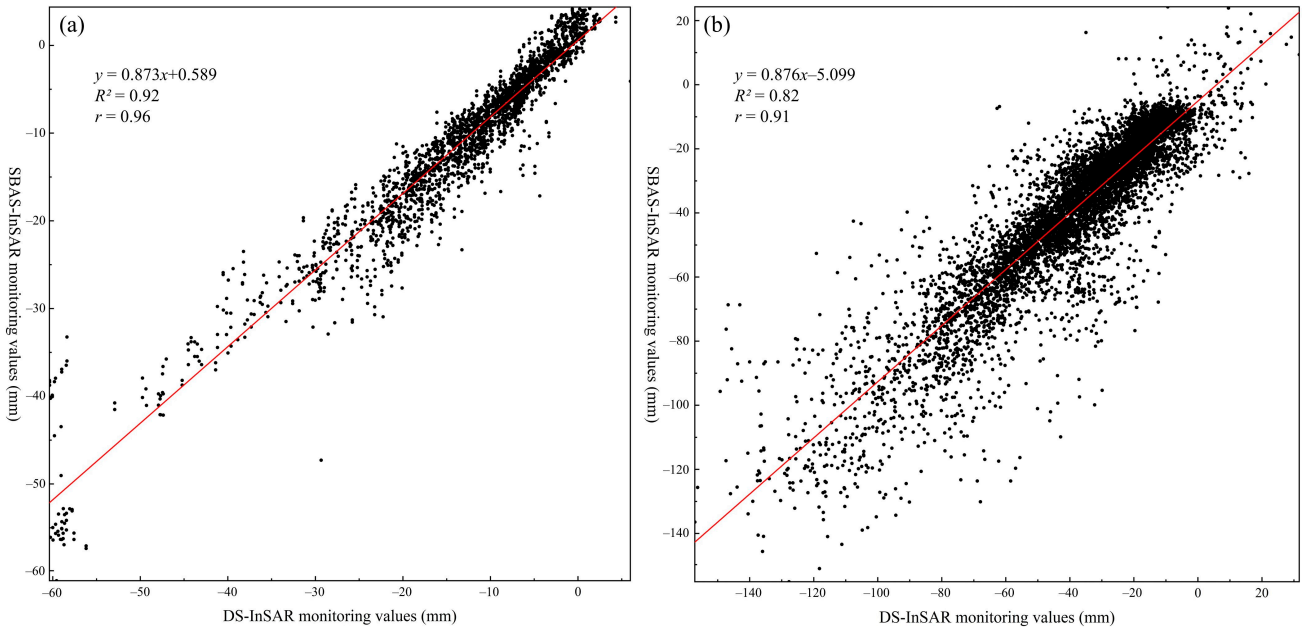

Figure 17. Scatter density maps of the mining areas in Wu'an (**a**) and Inner Mongolia (**b**).

6. Discussion

Our proposed method integrating DS-InSAR technology with UAV photogrammetry products overcame low accuracy issues for external reference DEMs and DS extraction in conventional DS-InSAR. It also achieved good application results in monitoring mining areas in Wu'an and Inner Mongolia, indicating the proposed method's strong applicability. While comparing the monitoring of the two mining areas, we found that different characteristics between the two mining areas brought about various changes in the process and results.

1. The impact of mining depth In the comparison of monitoring accuracy between the two mining areas, the monitoring error in the Wu'an mining area is considerably smaller than that in the Inner Mongolia mining area (Table 3). Based on established knowledge, with similar mining thicknesses, shallower mining depths tend to result in greater deformation but within a narrower range. Conversely, deeper mining depths lead to less deformation but over a broader area. In the cases of the experiments of two mining areas, the coal seam thickness in the Inner Mongolia mining area (3.3 m) is thinner compared to that in the Wu'an mining area (5 m), and the mining depth (200 m) is shallower than in the Wu'an mining area (550 m). As demonstrated through the subsidence results depicted in Figures 14b and 15b, it is evident that the deformation in the Inner Mongolia mining area is generally more pronounced than that in the Wu'an mining area. Another scholar has previously posited a correlation between coal seam depth and subsidence. In 2014, Farhad Howladar et al. [45] found that under different coal seam burial depths (200–440 m), maximum subsidence occurs in coal seams with a burial depth of less than 200 m, and minimum subsidence occurs in coal seams with a burial depth of greater than 440 m. To sum up, when the difference in coal seam thickness is not large, a shallower mining depth could cause greater deformation, and greater deformation will limit the monitoring effect of InSAR, leading to larger errors.
2. The impact of land cover In the process of refining the original DSCs of the two mining areas, the distribution of shrubs in the Wu'an mining area was relatively concentrated (see a_1 and a_2 in Figure 18a), while the distribution of shrubs in the Inner Mongolia mining area was chaotic and scattered (see b_1 and b_2 in Figure 18b), which made it more difficult to extract the shrub distribution area in the Inner Mongolia mining area, while it was less difficult to extract the shrub distribution area in the Wu'an mining

area. Therefore, different land cover types and distribution conditions could affect the degree of difficulty in the proposed point selection method.

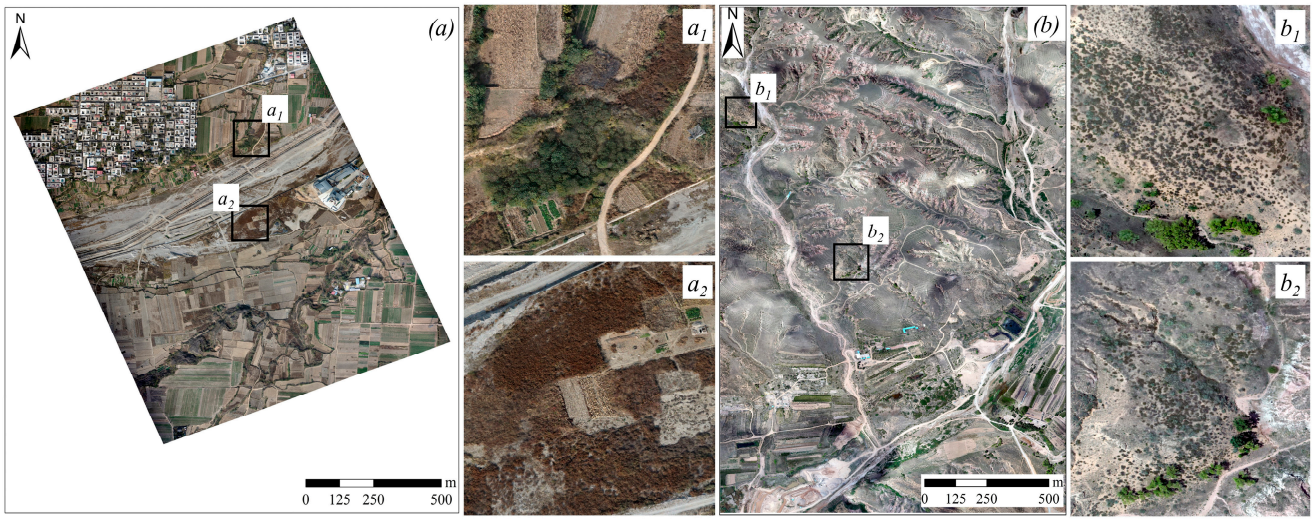

Figure 18. Comparison of shrub distribution in mining area in (**a**) Wu'an, Hebei, (**a**$_1$,**a**$_2$) show the details of black region in (**a**), respectively. (**b**) Inner Mongolia, (**b**$_1$,**b**$_2$) show the details of black region in (**b**), respectively.

3. The influence of topography The DS-InSAR results between the Wu'an and Inner Mongolia mining areas indicated distinct terrain characteristics. Wu'an exhibited a relatively flat topography, with deformation trends emanating from the center of the working face towards the surroundings. The farther one of these moved from the center, the less the deformation (Figure 14b). Conversely, Inner Mongolia's terrain was predominantly characterized by valleys, with higher elevations in the east and lower elevations in the west. The coal seam had an inclination angle of 2°, an influence that could be largely disregarded. Consequently, deformations on the east side of the working surface were less pronounced than those on the west side, leading to an irregular subsidence boundary (Figure 15b), which is related to the topography and terrain. Of course, this phenomenon may also be caused by factors such as the geological and structural background of the mining area [45], but due to different professions and the lack of data, it is hard to further investigate.

7. Conclusions and Outlook

7.1. Conclusions

DS-InSAR technology has great advantages in monitoring mining areas, but it has some limitations, including a lack of precision and the reliability of DS-InSAR monitoring results due to the insufficient precision of external reference DEMs and the low precision of DS extraction. Based on the obtained SAR images, UAV photogrammetry products (DEM and DOM), and data from field observation stations, we used two mining areas in Southeastern Wu'an and Northeastern Inner Mongolia as examples to propose a method for integrating UAV photogrammetry products with DS-InSAR and conduct comparative monitoring research on the two mining areas. We obtained more accurate and reliable subsidence results using the proposed method in two mining areas under different geomorphic and mining characteristics, which are as follows.

1. Although the mining depth could limit the monitoring effect of DS-InSAR, DS-InSAR technology uses a fused DEM as an external reference DEM, reducing monitoring errors better than the original DEM does and improving monitoring accuracy by 2 mm when it monitors mining areas under different mining depth conditions.
2. Based on the DS-InSAR monitoring results of two mining areas obtained via a fused external reference DEM, we compared monitoring accuracy results based on the points

of different ground types. We found that both mining areas showed the highest error for points with shrub ground types, indicating that non-DS points corresponding to the ground type (shrubs in this paper) cause poor monitoring accuracy.

3. The proposed DS selection method that integrates the high-resolution UAV DOM improved the number and density of points compared to those under traditional coherence threshold point selection. It did not exhibit low coherence due to the influence of the surface coverage type and large gradient deformation. Compared to conventional DS selection, it could eliminate non-DS points with low monitoring accuracy and increase the accuracy of point selection. Our method's application in the Wu'an and Inner Mongolia mining areas demonstrated a good point selection effect, indicating its strong applicability in mining environments of different surface types. However, difficulty in point selection depends on the surface coverage type and distribution of different mining areas.
4. Having compared the SBAS-InSAR and refined DS-InSAR results for the two mining areas, the monitoring accuracy of the latter's points is nearly the same as that of the former, but the latter has a higher number of points and a more uniform distribution. Therefore, it reflects the subsidence law of the mining area more comprehensively than does the former. After comparing the refined subsidence results for the mining areas in Wu'an and Inner Mongolia, we found that the topography could affect the mining area's deformation direction.

7.2. Shortcomings and Prospects

This paper utilized the advantages provided via UAV photogrammetry products and integrated them with those of DS-InSAR technology to obtain higher monitoring accuracy and more reliable mining subsidence results. However, the accuracy of vertical deformation is limited due to the use of only ascending SAR images. In addition, in the comparison of the precision of the refined DS-InSAR results, it was found that in areas with large gradient subsidence, due to the actual deformation exceeding the range that InSAR can monitor, there could be unwrapping errors, resulting in InSAR monitoring values being significantly lower than the actual deformation values. Furthermore, we did not conduct a temporal analysis of the settlement characteristics of the mining area's settlement results at the end of this paper. Therefore, there are many significant avenues of research for the future, which are as follows.

1. We will select a new experimental area in which to collect SAR data from various orbits, aiming to obtain more accurate vertical deformation to validate the reliability of the method proposed in this paper.
2. In order to compensate for the shortcomings of InSAR in large-gradient monitoring, the other technologies, such as UAV technology, fusion technology, DS-InSAR, etc., will be used to achieve high-precision monitoring in large-gradient-deformation areas.
3. We will select SAR data from the same period and process them separately using SBAS-InSAR and our proposed method, and compare the temporal subsidence feature changes of the two results, highlighting the advantages of the results obtained via the proposed method in temporal subsidence feature analysis.

Author Contributions: Conceptualization, J.Z., X.Y. and Y.N.; methodology, J.Z. and X.Y.; formal analysis, Y.N. and X.Y.; investigation, Y.N. and X.Y.; resources, Z.Z. (Zhaojiang Zhang); writing—original draft preparation, J.Z.; writing—review and editing, Y.N., X.Y., Z.Z. (Zhaojiang Zhang) and J.Z.; visualization, X.Y.; supervision, J.Z., Y.N. and Z.Z. (Zhaojiang Zhang); project administration, Y.N.; funding acquisition, J.Z. and Z.Z. (Zheng Zhao) All authors have read and agreed to the published version of the manuscript.

Funding: This research was supported by the Fundamental Research Funds for the Central Universities, grant number XJ2021005601; the National Key R&D Program of China, grant number 2022YFB3902605; the Natural Science Foundation of China (NSFC), grant number 42307255 and 41901286; the Technologies R&D Program from the Bureau of Science and Technology of Handan, grant number 21422903219; the Jiangsu Provincial Double-Innovation Doctor Program, grant number JSSCBS20221531.

Data Availability Statement: Research data would be shared from e-mail query.

Acknowledgments: Meanwhile, heartfelt thanks to the anonymous reviewers and the editors, whose comments and advice improve the quality of the work. We are grateful to USGS for providing the 1 arc-second SRTM DEM and ESA for providing Sentinel-1A/B. Thanks to DSIpro software package.

Conflicts of Interest: The authors declare no conflict of interest.

References

1. Wang, L.; Deng, K.; Zheng, M. Research on ground deformation monitoring method in mining areas using the probability integral model fusion D-InSAR, sub-band InSAR and offset-tracking. *Int. J. Appl. Earth Obs. Geoinf.* **2020**, *85*, 101981. [CrossRef]
2. Yang, Z.; Li, Z.; Zhu, J.; Yi, H.; Feng, G.; Hu, J.; Wu, L.; Preusse, A.; Wang, Y.; Papst, M. Locating and defining underground goaf caused by coal mining from space-borne SAR interferometry. *ISPRS J. Photogramm. Remote Sens.* **2018**, *135*, 112–126. [CrossRef]
3. Zhang, Q.; Huang, G.; Yang, C. Precision space observation technique for geological hazard monitoring and early warning. *Acta Geod. Cartogr. Sin.* **2017**, *46*, 1300–1307.
4. Malinowska, A.A.; Witkowski, W.T.; Guzy, A.; Hejmanowski, R. Mapping ground movements caused by mining-induced earthquakes applying satellite radar interferometry. *Eng. Geol.* **2018**, *246*, 402–411. [CrossRef]
5. Zhang, S.; Zhang, Y.; Yu, J.; Fan, Q.; Si, J.; Zhu, W.; Song, M. Interpretation of the spatiotemporal evolution characteristics of land deformation in beijing during 2003–2020 using sentinel, ENVISAT, and Landsat data. *Remote Sens.* **2022**, *14*, 2242. [CrossRef]
6. Zhang, B.; Wu, S.; Ding, X.; Wang, C.; Zhu, J.; Li, Q. Use of multiplatform SAR imagery in mining deformation monitoring with dense vegetation coverage: A case study in the Fengfeng Mining area, China. *Remote Sens.* **2021**, *13*, 3091. [CrossRef]
7. Carlà, T.; Intrieri, E.; Raspini, F.; Bardi, F.; Farina, P.; Ferretti, A.; Colombo, D.; Novali, F.; Casagli, N. Perspectives on the prediction of catastrophic slope failures from satellite InSAR. *Sci. Rep.* **2019**, *9*, 14137. [CrossRef] [PubMed]
8. Liu, G. *Principles and Applications of InSAR*; Science Press: Beijing, China, 2019.
9. Tao, W.; Jia, H.; Kang, M.; Liu, Y. Application of PS-InSAR method based on time series combination in surface deformation monitoring of Xiongxian county and its surrounding areas. *Bull. Surv. Mapp.* **2023**, *1*, 101–106.
10. Yang, C.; Zhang, D.; Zhao, C.; Han, B.; Sun, R.; Du, J.; Chen, L. Ground deformation revealed by Sentinel-1 MSBAS-InSAR time-series over Karamay Oilfield, China. *Remote Sens.* **2019**, *11*, 2027. [CrossRef]
11. Chaussard, E.; Wdowinski, S.; Cabral-Cano, E.; Amelung, F. Land subsidence in central Mexico detected by ALOS InSAR time-series. *Remote Sens. Environ.* **2014**, *140*, 94–106. [CrossRef]
12. Zhu, J.; Li, Z.; Hu, J. Research progress and methods of InSAR for deformation monitoring. *Met. Mine* **2017**, *46*, 1717–1733.
13. Wang, B.; Tan, Z.; Deng, K. Time series monitoring and analysis of surface subsidence in western mining areas based on DS-InSAR. *Met. Mine* **2022**, *5*, 160–169.
14. Liu, Y.; Yang, H.; Fan, J.; Han, J.; Lu, Z. NL-MMSE: A Hybrid Phase Optimization Method in Multimaster Interferogram Stack for DS-InSAR Applications. *IEEE J. Sel. Top. Appl. Earth Obs. Remote Sens.* **2022**, *15*, 8332–8345. [CrossRef]
15. Li, M.; Zhang, S.; Gao, Y. Optimized DS-InSAR technology for time series deformation monitoring in open-pit mines. *Met. Mine* **2023**, *1*, 110–118.
16. Chen, Y.; Li, J.; Li, H.; Gao, Y.; Li, S.; Chen, S.; Guo, G.; Wang, F.; Zhao, D.; Zhang, K. Revealing Land Surface Deformation over the Yineng Backfilling Mining Area, China, by Integrating Distributed Scatterer SAR Interferometry (DS InSAR) and a Mining Subsidence Model. *IEEE J. Sel. Top. Appl. Earth Obs. Remote Sens.* **2023**, *16*, 3611–3634. [CrossRef]
17. Jiang, J.; Du, Y.; Chen, Y.; Liu, G.; Yan, S. Monitoring and analysis of surface deformation in Peibei mining region based on DS-InSAR technique. *Bull. Surv. Mapp.* **2021**, *2*, 117.
18. Li, Y.; Jiang, J.; Du, Y.; Li, Z.; Yan, S. Surface subsidence monitoring by time series InSAR integrating with distributed targets in mining region. *J. China Univ. Min. Technol.* **2020**, *49*, 1199–1206.
19. Zhao, L. Research on Surface Deformation Monitoring Method in Mining Areas Based on DS-InSAR. Master's Thesis, China University of Mining and Technology, Xuzhou, China, 2022.
20. Tan, H. Research on the Law of Large Gradient Deformation in Mining Areas Based on the Fusion of Monitoring Data from the Space-Sky-Earth Platform. Doctoral Thesis, Anhui University of Science and Technology, Huainan, China, 2021.
21. Zhou, D.; An, S.; Wu, K.; Hu, Z.; Diao, X. Key technology and application of InSAR/UAV fusion monitoring for coal mining damages. *Coal Sci. Technol.* **2022**, *50*, 121–134.
22. Gao, Y.; Zhou, D.; An, S.; Wang, L.; Zhang, D.; Zhan, S. Study on surface subsidence in coal mining by UAV-photogrammetry monitoring technology. *Coal Sci. Technol.* **2022**, *50*, 57–65.

23. Di, M.; Zhang, L.; He, Y.; Xu, N.; Qiao, L.; Li, X. Deformation monitoring and analysis of Wu'an subsidence area based on SBAS-InSAR technology. *Geogr. Geogr. Inf. Sci.* **2021**, *37*, 52–56.
24. Li, W. Research on Land Subsidence Monitoring in Handan Mining Area Based on InSAR Technology. Master's Thesis, Shandong University of Science and Technology, Qingdao, China, 2019.
25. Yan, D. Application Research on Monitoring Mining Subsidence in Yunjialing Coal Mine Area Based on D-InSAR Technology. Doctoral Thesis, China University of Geosciences Beijing, Beijing, China, 2011.
26. Yadav, S.K.; Borana, S.L. Monitoring and temporal study of mining area of Jodhpur City using remote sensing and GIS. *Int. Res. J. Eng. Technol.* **2017**, *4*, 1732–1736.
27. Zhang, X. Research on Mining Area Subsidence Monitoring Method Based on UAV Photogrammetry Technology. Master's Thesis, Hebei University of Engineering, Handan, China, 2019.
28. Wang, R. Research on Multi-Source Data Fusion Technology and Application for Mining Subsidence Monitoring. Doctoral Thesis, China University of Mining and Technology, Xuzhou, China, 2022.
29. Zhou, L.; Li, Q.; Quan, F.; Wei, L.; Liao, J. 3D model and accuracy evaluation of tilt photogrammetry based on UAV. *Water Power* **2020**, *46*, 41–45+50.
30. Chen, Q.; Yuan, Y.; Fu, X.; Zhang, W.; Dong, X. Application of UAV photogrammetry technology in emergency investigation of Aniangzhai landslide. *Bull. Surv. Mapp.* **2023**, *1*, 77–83+119.
31. Du, Y.; Yan, S.; Yang, H.; Jiang, J.; Zhao, F. Investigation of deformation patterns by DS-InSAR in a coal resource-exhausted region with Spaceborne SAR imagery. *J. Asian Earth Sci. X* **2021**, *5*, 100049. [CrossRef]
32. DSIpro. Available online: http://mijiang.org.cn/index.php/software/ (accessed on 9 October 2023).
33. Peng, K. Research on DS-InSAR Surface Deformation Monitoring in Fukang Coalfield Fire Area, Xinjiang. Master's Thessis, China University of Mining and Technology, Xuzhou, China, 2021.
34. Lu, L. Research on DS-InSAR Method for Monitoring Surface Time Series Subsidence in Mining Areas. Master's Thesis, China University of Mining and Technology, Xuzhou, China, 2020.
35. Liu, Y. Research on Surface Subsidence Monitoring Method for Filling Mining Area Based on DS-InSAR. Master's Thesis, China University of Mining and Technology, Xuzhou, China, 2021.
36. Zhu, J.; Hu, J.; Li, Z.; Sun, Q.; Zheng, W. Recent progress in landslide monitoring with InSAR. *Acta Geod. Cartogr. Sin.* **2022**, *51*, 2001–2019.
37. Wu, H.; Fan, H.; Zheng, C.; Liu, J. Deformation monitoring and analysis of Tailings Dam based on DS-InSAR: A case study of Brumadinho Mine in Brazil. *Met. Mine* **2023**, *3*, 169–176.
38. Liu, Y.; Fan, H.; Wang, L.; Zhuang, H. Monitoring of surface deformation in a low coherence area using distributed scatterers InSAR: Case study in the Xiaolangdi Basin of the Yellow River, China. *Bull. Eng. Geol. Environ.* **2021**, *80*, 25–39. [CrossRef]
39. Wu, S.; Wu, W.; Long, S.; Zhang, T. Application of distributed targets in deformation monitoring of Hongqinghe Coal Mine. *J. Geod. Geodyn.* **2019**, *39*, 1261–1264.
40. Li, Z.; Zhu, W.; Yu, C.; Zhang, Q.; Zhang, C.; Liu, Z.; Zhang, X.; Chen, B.; Du, J.; Song, C. Interferometric synthetic aperture radar for deformation mapping: Opportunities, challenges and the outlook. *Acta Geod. Cartogr. Sin.* **2022**, *51*, 1485–1519.
41. Ferretti, A.; Fumagalli, A.; Novali, F.; Prati, C.; Rocca, F.; Rucci, A. A new algorithm for processing interferometric data-stacks: SqueeSAR. *IEEE Trans. Geosci. Remote Sens.* **2011**, *49*, 3460–3470. [CrossRef]
42. Li, P. A Study on the Interseismic Strain Accumulation in the Western Section of the Altyn Tagh Fault Zone Observed by Wideband InSAR. Doctoral Thesis, Wuhan University, Wuhan, China, 2013.
43. Wang, Y.; Wang, L.; Li, J.; Jiang, K.; Li, S.; Yang, K.; Liu, H. Full-scale gradient surface deformation monitoring in mining area based on LEV-InSAR model. *Met. Mine* **2023**, *1*, 134–141. [CrossRef]
44. Li, Z.; Song, C.; Yu, C.; Xiao, R.; Chen, L.; Luo, H.; Dai, K.; Ge, D.; Ding, Y.; Zhang, Y. The application of satellite radar remote sensing in landslide disaster detection and monitoring: Challenges and countermeasures. *Geomat. Inf. Sci. Wuhan Univ.* **2019**, *44*, 967–979.
45. Howladar, M.F.; Hasan, K. A study on the development of subsidence due to the extraction of 1203 slice with its associated factors around Barapukuria underground coal mining industrial area, Dinajpur, Bangladesh. *Environ. Earth Sci.* **2014**, *72*, 3699–3713. [CrossRef]